Towards a consistent model of the Galaxy

I. Kinematic properties, star counts and microlensing observations

D. Méra[1,3]**, G. Chabrier**[1]**, and R. Schaeffer**[2]

[1] C.R.A.L. (UMR CNRS 5574), Ecole Normale Supérieure, F-69364 Lyon Cedex 07, France,
[2] Service de Physique Théorique, CEA Saclay, F-91191 Gif-sur-Yvette, France
[3] Physics Department, Whichita State University, 1845 Fairmount, Wichita KS 67260, USA

Abstract. We examine the most recent observational constraints arising from i) small-scale and large-scale Galactic dynamical properties, ii) star counts of population I and II stars at faint magnitude and iii) microlensing experiments towards the Large Magellanic Cloud and the Galactic centre. From these constraints, we determine the halo and disk stellar mass functions and stellar content down to the bottom of the main sequence, which yields the normalization of the halo/disk *total* stellar population, and we infer the contributions of sub-stellar objects to the mass budget of the various Galactic regions.

The consistent analysis of star counts and of the *overall* microlensing observations in the bulge are compatible with a small contribution of brown dwarfs to the Galactic mass budget $\rho_{\mathrm{BD}}/\rho_* \leq 0.2$. However the *separate* bulge/disk analysis based on the bulge clump giants is compatible with a substantial population of disk brown dwarfs, $\Sigma_{\mathrm{BD}}/\Sigma_* \leq 1$. The most recent determination of the disk surface density, that lies within one standard deviation of all previous measurements, allows such a maximum brown dwarf contribution at the 1σ level. More statistics of microlensing events towards the Galactic center and a better determination of the velocity dispersions in the bulge should break this degeneracy of solutions.

For the halo, we show that a steep mass-function in the dark halo is excluded and that low-mass stars and brown dwarfs represent a negligible fraction of the halo dark matter, and thus of the observed events towards the LMC. The nature of these events remains a puzzle and halo white dwarfs remain the least unlikely candidates.

Key words: stars: low-mass, brown dwarfs – Galaxy: stellar content – Galaxy: halo – cosmology: dark matter

1. Introduction

There is compelling evidence for believing that most of the matter in the Universe is under the form of dark, yet unobserved components. The observed density of baryons in galaxies $\Omega_{\mathrm{star+gas}} \sim 0.003\,h^{-1}$ (h is the Hubble constant in units of 100 km.s^{-1} Mpc^{-1}) may represent only a fraction of the value predicted by primordial nucleosynthesis, $\Omega_B \approx 0.01\,h^{-2}$ (Copi, Schramm & Turner, 1995). There is also evidence that spiral galaxies are surrounded by a large amount of non-luminous mass of unknown nature. These two facts suggest that baryonic dark matter is a possible candidate for halo dark matter. A breakthrough in this longstanding, unsolved problem has been accomplished recently with the developement of microlensing experiments, by inferring the presence of dark objects through their gravitational effect on luminous matter. The analysis of the EROS (Aubourg et al., 1993; Ansari et al., 1996) and MACHO (Alcock et al., 1993; 1996) observations towards the LMC, in particular, reveal the presence of *some* baryonic matter in the Galactic halo, although the inferred optical depth shows that this dark baryonic matter probably does not provides *all* the sought missing mass. On the other hand, microlensing experiments towards the central regions of the Galaxy yield a mass density of unseen star-like objects about three times larger than the value expected from standard disk+bulge models (Udalski et al. 1994; Alcock et al., 1997). These two results from microlensing experiments - the lack of events in the halo and the excess of events in the bulge - lead to the tempting conclusion that more (resp. less) galactic dark matter than expected previously resides in the disk (resp. the halo). On the other hand, severe constraints on the amount of dark matter in the disk and in the halo arise from the observed large-scale kinematic properties, i.e. the rotation curve of the Galaxy at distances larger than the observed luminous distribution, as well as from the small-scale dynamical properties, i.e. the stellar velocity dispersion in the solar neighborhood. This latter information is derived from the measurement of the vertical acceleration due to the galactic potential near the Sun, which yields the determination of the local dynamic surface density. Finally, star counts have now been obtained at very faint magnitudes, either from the HST or from ground-based deep-magnitude surveys, and provide stringent constraints on different parameters entering galactic modeling

such as scale lengths, scale heights, and more indirectly stellar mass functions.

These two latter type of constraints, galactic dynamics and star counts, have usually suggested that most of the Galactic missing mass resides in the outer so-called dark halo. There is then an apparent conflict between the afore-mentioned microlensing results and standard astronomical observations. This paradigm stresses the need to reconsider the standard model of the Galaxy, where all dark matter resides in the halo, and to derive a Galactic mass-model consistent with the three types of observational constraints, kinematics, star counts and microlensing. This is the aim of the present study.

The calculations will be presented in two joint papers. In the present one (Paper I), we examine in detail all observational constraints arising from the most recent determinations of small-scale and large-scale Galactic dynamic properties (§2), from star counts in the Galactic disk, bulge and spheroid (§3), and from microlensing experiments towards both the Large Magellanic Cloud (LMC) and the Galactic center (§4). A *consistent analysis* of all these observations yields the determination of the stellar mass functions, slope, normalization and minimum mass, and thus of the amount of mass under the form of stellar and substellar objects in the various regions of the Galaxy, disk, bulge, spheroid and dark halo.

In Paper II, these results will be used to derive a consistent model for the Galaxy, confronted to all types of observational constraints. We will discuss in detail the two possibilities of an essentially non-baryonic and a dominantly baryonic mass model for the Galaxy (Méra, Chabrier & Schaeffer, 1997).

2. Kinematic constraints

In this section we examine the most recent observational determinations of the kinematic properties of the Galaxy. We first consider the asymptotic circular velocity, in the Milky Way and in other spiral galaxies, and then the velocity distribution in our Galaxy up to 60 kpc. Different determinations of the total *mass* of the Galaxy, converted into equivalent circular rotation velocities $v_{rot}^2 = GM(r)/r$, are also examined. In the second part of this section, we focus on the determination of the local surface density, inferred from the measurement of the gravitational acceleration of the Galactic potential near the Galactic mid-plane. From all these observations, we derive the most likely values for the Galactic mass, rotation velocity, and amount of dark matter near the Sun, to be reproduced by the final galactic model.

2.1. Large scale velocities

2.1.1. Circular velocity

The most recent determinations of the circular velocity as a function of the Galactic radius have been reviewed by Fich and Tremaine (1991). Their compilation of the measurements of the outer rotation curve from CO, HI and HII observations yields the accurate determination of a velocity of about 220 km.s^{-1}, constant within ~10% up to 14 kpc, with extremely small error

bars (a few %). At larger distance there is a hint for a small increase of the rotation curve, but the uncertainty in the data does not allow any robust conclusion. In any case, there is no sign for a significant decrease of the velocity up to about 20 kpc. More recent observations of neutral hydrogen out to 2.5 $R_{\odot}$, where $R_{\odot} \sim 8$ kpc is the galactocentric position of the Sun, yield a slightly lower value $v_{rot} = 200 \pm 10$ km.s^{-1} (Merrifield, 1992). On the other hand, Schechter et al (1989) report $v_{rot} = 248 \pm 16$ km.s^{-1} from the kinematics of carbon stars in the outer Galaxy. As noted by Kuijken & Tremaine (1994), a difference between the value determined from stellar and HI tracers is expected, because of the ellipticity of the galactic potential. This will decrease the afore-mentioned stellar value.

The determination of the rotation curves of external galaxies (Casertano and Van Albada 1990) characterizes what these authors call "bright galaxies", with circular velocities bracketed between 180 and 260 km.s^{-1}. These rotation curves show occasionally a slight drop beyond 20 kpc, which for all of them remains within less than 20% at 35 or 40 kpc, almost within the error bars. The rotation curves are thus flat within the error bar determination ($\sim 10 - 20\%$) up to the furthest distance at which hydrogen is detectable, i.e more than twice the radius of the visible stellar component. Although no rotation velocity measurements exist for our Galaxy beyond 19 kpc, Fich and Tremaine (1991) argue that, by comparison with other galaxies, our rotation curve should extend similarly up to at least 35 kpc.

Note that the Galactic rotation is well confined to the disk plane. At 1 kpc above the disk, metal-rich stars show similar rotation velocities and are considered as belonging to the (thick) disk population. Most of the metal-depleted stars ($[Fe/H] < -1.5$), which probe essentially the halo population, rotate only with $\sim 30-40$ km.s^{-1} assuming a rotation velocity 220 km.s^{-1} for the Local Standard of Rest, arguing for a non-rotating, or slowly rotating halo (Beers and Sommer-Larsen, 1995).

2.1.2. Velocity distribution up to 60 kpc

Attempts to determine the gravitational potential of our Galaxy at large distances, from the study of the motion of globular clusters, require some modelling of the velocity distribution in the Galactic halo, which enters the Jeans equation (Binney & Tremaine 1987). The compilation of Harris and Racine (1979) led Frenk and White (1980) to use a 66 cluster sample, with various assumptions for the shape of the Galactic halo, to determine the mass of the Galaxy within 33 kpc. These clusters show an overall 60 ± 26 km.s^{-1} circular rotation (assuming $v_{lsr} = 220$ km.s^{-1}), again advocating for a slow rotation of the halo, but also for important non-circular motion. Translating the dynamically measured mass of the halo within a given radius into an effective circular rotation velocity ($v_{rot}^2 = GM/R$), their results can be summarized as follows: this velocity always lies within the range $200 \leq v \leq 319$ km.s^{-1}, for *all* models, at the 90% confidence level. With the additional constraint that the globular cluster distribution is not more flattened in the outer region than in the inner region, the allowed velocity-range reduces to 200-265 km.s^{-1}. A second restriction stems from the

fact that if the velocity distribution is not isotropic, the radial rms velocity σ_r must be larger than the tangential velocity v_t, because of infall towards the centre of the Galaxy. This leads to the final range $224\,\mathrm{km.s^{-1}} < v_{\mathrm{rot}}(33\,\mathrm{kpc}) < 265\,\mathrm{km.s^{-1}}$, the uncertainty being due to systematic errors.

The more distant the constraint, the more relevant it is to determine the dark matter content of the Galaxy, but the more uncertain the data. The sample of 17 globular clusters and dwarf spheroidal galaxies at galactocentric distances from 20 up to 60 kpc has been analysed by Hartwick and Sargent (1978). They determine the mass within 60 kpc, under the two opposite extreme assumptions of purely radial or purely isotropic velocity distributions, respectively. Translated into a circular velocity, this leads respectively to $v_{\mathrm{rot}} = 159 \pm 30\,\mathrm{km.s^{-1}}$ and $v_{\mathrm{rot}} = 237 \pm 30\,\mathrm{km.s^{-1}}$. Caldwell and Ostriker (1981) used the more realistic geometrical mean of the two values $v_{\mathrm{rot}} = 192 \pm 42\,\mathrm{km.s^{-1}}$. The latter finally has been scaled by Bahcall et al (1983) to $v_{\mathrm{rot}}(60\,\mathrm{kpc}) = 205\,\mathrm{km.s^{-1}}$ (to which must be added a ±45 km.s^{-1} uncertainty) in order to take into account more recent determinations of the local parameters near the Sun. These results are consistent with the more recent and much more precise (although requiring a modelling of the galaxy profiles) determination of the mass of the Galaxy by Kochanek (1996), i.e. $3.8 \times 10^{11}\,\mathrm{M_\odot} < M_{30} < 5.4 \times 10^{11}\,\mathrm{M_\odot}$ and $4.0 \times 10^{11}\,\mathrm{M_\odot} < M_{60} < 8.7 \times 10^{11}\,\mathrm{M_\odot}$ at the 90% C.L., where M_{30} and M_{60} denote the mass within 30 and 60 kpc, respectively. This yields, within the 1σ error level we have been using all along the present analysis, $v_{\mathrm{rot}}(30) = 257 \pm 8$ km.s^{-1} and $v_{\mathrm{rot}}(60) = 210 \pm 13$ km.s^{-1}.

Fich and Tremaine (1991) discuss the implications of the velocities measured for the "Magellanic Stream", a hydrogen bridge between the Magellanic Clouds and the Galaxy. A detailed modelling shows that the r^{-2} ($r^{-1.8}$ fits better) halo should extend up to at least 60 kpc. Although such a conclusion is reached by means of several "natural" assumptions, and may be questioned, the raw data show gas velocities around 200 km.s^{-1}.

Peebles (1989, 1990, 1994) has examined the total mass of the Local Group, dominated by Andromeda and the Milky Way. He finds total masses around $4 \times 10^{12}\,\mathrm{M_\odot}$, suggesting a total mass of about $2 \times 10^{12}\,\mathrm{M_\odot}$ for our Galaxy. Moreover, a modelling of all objects at a distance of 4 Mpc from the Galaxy shows indeed that their velocity distribution is consistent with the mass being attached to the objects.

In summary, all these studies lead to the conclusion that the Milky Way has a mass $M_G \approx 2 \times 10^{12}\,\mathrm{M_\odot}$, with a nearly constant rotation velocity $v_{\mathrm{rot}} = 220 \pm 20$ km.s^{-1}, which implies an extension of a Galactic dark halo up to at least 100 kpc. This undetected mass has to be compared with the mass under the form of visible matter, $\sim 10^{11}\,\mathrm{M_\odot}$, which sets the scale for the amount of dark matter in the Galaxy.

2.2. Local dynamical surface density

An important constraint on the mass density of the Galactic disk in the solar neighbourhood is obtained from the study of the vertical acceleration K_z by means of the local stellar velocity distribution. $K_z(z)$ is related to the (measured) vertical velocity dispersion $\langle v_z^2 \rangle$ and density of one tracer population (Binney & Tremaine,1987) by:

$$K_z(z) = -\frac{1}{\rho}\frac{\partial \rho \langle v_z^2 \rangle}{\partial z} \tag{1}$$

By Taylor-expanding the Galactic potential above the disk, $\Phi(z) \approx K_z z + F z^2$, the Poisson-Jeans equation yields (Binney & Tremaine 1987):

$$K_z(z) = \frac{\partial \Phi}{\partial z} = K_{z0} + 2zF \tag{2}$$

where the coefficient K_{z0} depends on the mass content in the disk (assumed to be infinitely thin, which means the above expression is good for $z \gtrsim 300$ pc only) while $F = 2\pi G \rho_{halo}$ is the halo contribution. The local surface density $\Sigma_\odot$ in the disk is related to K_{z0} by:

$$\Sigma_\odot = \frac{K_{z0}}{2\pi G} \tag{3}$$

The surface density near the Galactic mid-plane determines the mass of the disk, for a given disk scale length R_d:

$$M_{\mathrm{disk}} \approx 2\pi \Sigma_\odot R_d^2 \, e^{R_\odot/R_d} \tag{4}$$

In practice, $K_z(z)$ is measured at some height z and must be corrected from the halo contribution $2zF$ to determine K_{z0} and $\Sigma_{\odot\mathrm{disk}}$. Bahcall (1984a, 1984b), in agreement with Oort (1960) found $\Sigma_\odot \approx 70\,\mathrm{M_\odot\,pc^{-2}}$ with a claimed small error. Bienaymé, Robin and Crézé (1987), using a sampling extending to higher latitudes, obtained a better determination of $K_z(z)$ from 100 pc to 1 kpc, based on a modelling of the disk and the halo stellar population arising from available observations. They found a lower surface density for the disk,

$$\Sigma_\odot = 50\,\mathrm{M_\odot\,pc^{-2}}, \tag{5}$$

with a $10\,\mathrm{M_\odot\,pc^{-2}}$ uncertainty, and stressed that the uncertainties in Bahcall's extrapolation to low z were underestimated. These authors, however, actually measure the acceleration at 1 kpc, where the surface density is essentially the *total* surface density, and get $K_z(1\,\mathrm{kpc})/2\pi G \approx 70\,\mathrm{M_\odot\,pc^{-2}}$. The aforevalue of $\Sigma_\odot$ quoted for the disk is obtained after substracting the standard halo contribution[1] (see Eq. (2)), and thus becomes model-dependent. Subsequently, Kuijken and Gilmore (1989, 1991), found an observed *total* density $\Sigma(1.1\,\mathrm{kpc}) = 71 \pm 6$ $\mathrm{M_\odot\,pc^{-2}}$ and argued that, after a theoretical correction for the contribution of a standard massive halo similar to the one used

---

[1] Throughout this paper, the *standard* halo is defined as a halo with a density profile $\rho(r) = \frac{v_{\mathrm{rot}}^2}{4\pi G}\frac{R_\odot^2 + R_c^2}{r^2 + R_c^2}$, with $v_{\mathrm{rot}} = 220$ km.s^{-1} and $R_c = 5$ kpc, see Paper II. Note that this halo is slightly heavier than the one used for instance by the MACHO group, which corresponds to $v_{\mathrm{rot}} = 204$ km.s^{-1}.

by Bienaymé et al. (1987), the surface density of the disk should be reduced to:

$$\Sigma_\odot = 48 \pm 9 M_\odot \, pc^{-2}, \tag{6}$$

in remarkable agreement with the afore-mentioned determination. A subsequent reanalysis of the Kuijken & Gilmore (1989) work gives in fact $\Sigma_\odot = 54 \pm 8 \, M_\odot \, pc^{-2}$ (Gould, 1990). We stress, however, that the two afore-mentioned surface densities at 300 pc depend somehow on the assumption made for the dark halo contribution (Eq. (2)).

More recently, Bahcall, Flynn and Gould (1992), using the new data of Flynn and Freeman (1993), re-analyzed Bahcall's (1984) previous determination, and obtained

$$\Sigma_\odot = 85 \pm 25 M_\odot \, pc^{-2}. \tag{7}$$

The new lower limit weakens substantially the conflict with the afore-mentioned values, at the price however of a large uncertainty. The most recent analysis of these data by Flynn and Fuchs (1994), who added a new normalization point, yields a best fit model:

$$\Sigma_\odot = 52 \pm 13 \, M_\odot \, pc^{-2} \tag{8}$$

Both groups include a standard halo contribution in their determination but for the average height of their sample (~ 300 pc), the halo correction is small ($\sim 6 M_\odot \, pc^{-2}$) and the associated uncertainty lies well within the observational error bars. The reason why Bahcall et al. (1992) considered their value to disagree significantly with the Bienaymé et al. (1987) and Kuijken & Gilmore (1991) values is that even with a 1σ deviation, the probability for $\Sigma_\odot$, as given by (7), to be less than $60 M_\odot \, pc^{-2}$ is only 7% and thus has only one chance in 14 to occur, as stated by these authors. More optimistically, comforted by the recent Flynn & Fuchs (1994) result, we note that all these determinations of $\Sigma_\odot$ should rather be considered as consistent at the 1σ level: the uncertainty-weighted average of these four different results (5)-(8) yields:

$$\Sigma_\odot = 51 \pm 6 \, M_\odot \, pc^{-2}, \tag{9}$$

very close to Eq. $(8)^2$. We thus may consider the value (8) as the most accurate present determination of the solar dynamical density.

3. Star counts

3.1. Disk

The determination of the faint end of the stellar luminosity function (LF), an essential issue to infer the low-mass star and the sub-stellar contributions to the Galactic mass budget, has also been subject to strong debate. Wielen et al. (1983) found that,

whereas the LF was steadily rising up to $M_V = 13$, there was a dip beyond this value, leaving very little possibility for a substantial contribution of low-mass stars to the mass of the disk. Subsequent studies (Stobie et al. 1989, Tinney et al. 1992) showed that the dip is even more pronounced and starts already at $M_V = 12$. Gould, Bahcall and Flynn (1996;1997), using HST observations at faint magnitudes, confirm a dropping LF beyond $M_V = 12$, which corresponds to $m \sim 0.25 \, M_\odot$, although the last bin of the HST LF clearly shows an upturn at $M_V > 16$. Most of these LFs are based on a photometric determination of the distance, which thus relies on a color-absolute magnitude relationship, up to about a few hundred pc. On the other hand, Kroupa (1995) used a nearby LF, allowing a *geometric* determination of the distance. This yields larger statistical errors, due to the number-limited sample, but better systematic corrections, in particular the ones arising from the unresolved binary companions. The nearby LF agrees with the photometric one up to $M_V \sim 12$ but is essentially flat beyond this limit. Doing a careful correction for the Malmquist bias and for the presence of unresolved binaries, Kroupa, Tout and Gilmore (1990; 1993) and Kroupa (1995) have shown that the properly corrected ground-based photometric LFs are consistent with the local geometric LF.

The issue, however, remains unsettled for the HST LF (Gould et al., 1996; 1997). The HST is almost not subject to Malmquist bias since its limit magnitude allows the observation of the bottom of the main sequence up to the edge of the disk, but it is subject to uncompleteness due to unresolved systems near the faint end[3]. Gould et al. (1997), however, found that even with this correction, their LF is inconsistent with the nearby LF. Near the end of the LF, the binary correction is, according to these authors, at most a factor 2, whereas a factor ~ 5 is required to reconcile the two kinds of LFs. Therefore, unresolved binaries are certainly not the source of the discrepancy between the two LF's. An important quantity to calculate correctly the correction due to binaries is the rate of binaries and the mass-distribution of the secondaries. An accurate determination of such quantities require decade-long observations, as conducted for example by Duquennoy and Mayor (1991; DM91) for nearby F and G stars, with a fairly accurate sensitivity ($\sim 300 \, m.s^{-1}$). Note that, although there are severe natural observational biases toward the detection of near equal-mass systems either from imaging or from spectroscopic surveys, the completeness and the uniformity of the DM91 sample render it almost without any observational selection effect, yielding an almost unbiased mass-ratio determination for F and G star binaries. The main conclusion of the DM91 study is that a fairly large number ($\sim 60 - 70\%$) of single stars form a multiple system, and that the shape of the mass-distribution increases toward small mass ratios ($q = m_2/m_1 < 1$; see their Fig. 10).

M-dwarf surveys to address the same issue are still in their infancy and suffer from severe incompleteness and observational biases, so that it will require more years to do a similar

---

[2] Strickly speaking, the Bahcall et al. (1992) and the Flynn & Fuchs (1994) values are not completely independent but the weight of the Bahcall et al. value is small. In any event, the value used as a reference all along our calculations is the most recent Flynn & Fuchs one.

---

[3] The HST is insensitive to binaries with separations $\lesssim 0.''3$ and thus misses essentially all secondaries in late M-dwarf binary systems.
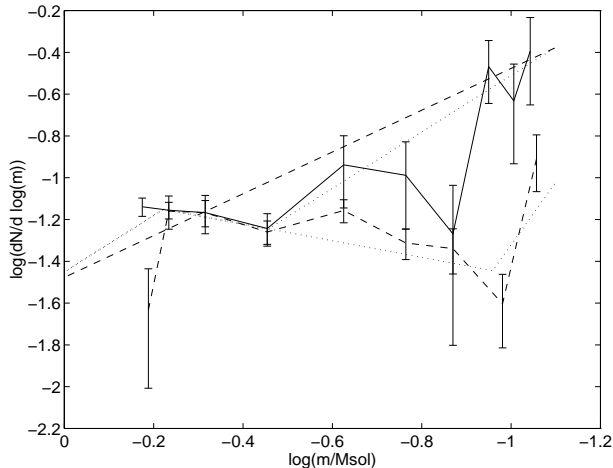
Fig. 1. Mass functions derived from Kroupa (1995; solid line) and Gould et al. (1997; dashed line) LFs. Also shown are the fits for both MFs, which are identical for $m > 0.35 M_\odot$ (dotted lines). See table 1 for the parameters of the fits. The dashed line is an overall fit given by Eq. (10) with $\alpha = 2$, which reproduces reasonably well the MF derived from Kroupa's LF (note that there are only 2 stars in the lowest bin of Kroupa's LF; see text).

Table 1. Fit of the two MFs considered in this paper. The MF (a) has been derived from Kroupa (1995) LF, whereas the MF (b) has been derived from Gould et al. (1997) LF. The MFs and their fits are displayed in Fig. 1. Each MF is considered to be a 3-segment power-law $\mu(m) = dN/dm = A\, m^{-\alpha}$. Both MFs are identical for $m > 0.35\,M_\odot$. The mass is in $M_\odot$, the mass function in $M_\odot^{-1}\,pc^{-3}$. The upper mass limit has been set arbitrarily to $10\,M_\odot$, since it has almost no influence on the mass density. Note that 0.4 should be added to the slope derived from the HST LF for $m < 0.6\,M_\odot$ to account for missed binaries (Gould et al., 1997)

MF (a):			
mass	$m_{\rm inf} - 0.35$	$0.35 - 0.6$	$0.6 - 10$
α	2.35	0.6	2.35
A	5.98×10^{-3}	3.76×10^{-2}	1.54×10^{-2}
MF (b):			
mass	$m_{\rm inf} - 0.11$	$0.11 - 0.6$	$0.6 - 10$
α	4	0.6	2.35
A	2.08×10^{-5}	3.76×10^{-2}	1.54×10^{-2}

analysis for M-dwarf binaries. In any case, as mentioned above, even a full knowledge of the binary correction will not account for all the discrepancy between photometric and geometric LFs. For this reason, we have considered in the present paper both (nearby and HST) LFs.

We have converted both LFs into *mass-functions* (MF), using low-mass star models which accurately reproduce observed mass-M_V relationships (Chabrier, Baraffe & Plez, 1996). Both MFs are displayed in Fig. 1 in a log-log scale. The aforementioned discrepancy between the two LFs is obvious on the MF, in particular in the domain $\sim 0.1 - 0.25\,M_\odot$, with a factor ~ 5 ratio at $\sim 0.1\,M_\odot$.

Noting that the two lowest bins in the nearby LFs are the least statistically significant (2 stars, see Kroupa (1995)), Méra et al. (1996a) parametrized the disk low-mass star MF in the solar neighborhood down to the vicinity of the hydrogen-burning limit by the following form:

$$\mu(m) \approx 1.5 \pm 0.4 \left(\frac{m}{0.1\,M_\odot}\right)^{-2 \pm 0.5} M_\odot^{-1}\,pc^{-3}, \qquad (10)$$

The undetermination of the exponent reflects the fact that this fit is a *reasonnable* overall power-law representation of the true MF but is not perfect. As shown by Kroupa et al. (1993), the MF determined from the nearby LF is better described by a series of segment power-law fonctions $\mu(m) = dN/dm \propto m^{-\alpha}$. We then have fitted the MFs derived from the nearby and the HST LFs with such segmented power-laws. The characteristics of these MFs are given in table 1 and illustrated in Fig. 1. We will refer to these fits as MF (a) for Kroupa (1995) and MF (b) for Gould et al. (1997).

If we exclude the last bin, the HST MF corresponds to a slope $\alpha < 1.0$ for $m/M_\odot \lesssim 0.6$. However, an extrapolation of

the MF (ignoring the last bin) all the way below $0.2\,M_\odot$ would correspond to about 2 stars in the last bin whereas 10 are seen. The probability to see 10 stars whereas 2 are expected is less than 5×10^{-5}. This suggests that the last bin in the HST LF is indeed significant, adding credibility for a rising MF near the BD limit. As shown in Fig. 1, the fit does not reproduce exactly the last bin. This takes into account a possible bias which tends to overestimate the last bin and to underestimate the penultimate one (Gould et al. 1997).

Indeed, for both MF's (nearby and HST), there is a hint for a rise near 0.1 Msol, suggesting the possibility for a substantial amount of brown dwarfs in the disk. We will take this as a basis for extrapolating the stellar MF into the brown dwarf domain. This is consistent with a recent study by Mazeh, Latham & Stefanik (1996) on the distribution of secondary masses near the substellar limit. Although this study relies on the detection of 3 very-low-mass companions out of 20 F and G dwarfs and subgiants, and thus preclude the precise determination of a substellar MF, these detections suggest that the mass distribution (the primaries of the sample all have $\sim 1\,M_\odot$) rises near the sub-stellar limit.

In any case, whereas the precise determination of the shape of the MF near the bottom of the main sequence, which requires larger statistics, is of prime importance for star-formation theory, the qualitative behaviour, and its overall characterization, is what is most essential to estimate the stellar and sub-stellar mass contributions to the disk mass budget. Both rising MF's near the BD limit suggest a substantial amount of substellar objects and thus a contribution to the disk mass density. The extension into the brown dwarf domain will be analyzed in the next section, in connection with microlensing observations.

The integration of the nearby MF displayed in Fig. 1 gives the local low mass star ($0.07 M_\odot \leq m \leq 0.65 M_\odot$) densities $\rho_{\rm LMS} = 2.56 \pm 0.25 \times 10^{-2}\,M_\odot\,pc^{-3}$ in case (a), and $\rho_{\rm LMS} = 1.43 \pm 0.09 \times 10^{-2}\,M_\odot\,pc^{-3}$ in case (b). Since the HST LF does not include companions of multiple systems, we have tentatively corrected for this bias on the basis of the

Duquennoy and Mayor (1991) observed mass ratio distribution mentionned above. The correction is approximated by a a linear fonction, whose value is 10% at 0.6 $M_\odot$, and 80% at 0.1 $M_\odot$. We renormalize the HST MF to keep the same normalization at 0.6 $M_\odot$ with this correction. The resulting density is $\rho_{\rm LMS} = 1.88 \times 10^{-2}$ $M_\odot$ pc^{-3}, almost in agreement with the nearby value. An average value is then:

$$\rho_{\rm LMS} = 2.2 \pm 0.3 \times 10^{-2} \, M_\odot \, {\rm pc}^{-3}$$

With a vertical sech^2 density profile of scale height $h_d \approx 320$ pc (Gould et al., 1997), the contribution of low-mass stars (LMS) down to the bottom of the main sequence ($0.1 \lesssim m/M_\odot \lesssim 0.6$) to the disk surface density is then:

$$\Sigma_{\rm lms} \approx 14 \pm 2 \, M_\odot \, {\rm pc}^{-2} \tag{11}$$

Adding the contribution of more massive stars, obtained with the MF and the luminosity-dependent scale height determined by Miller & Scalo (1979), converted into a mass-dependent scale height, yields the total contribution of main sequence stars:

$$\Sigma_\star = 24 \pm 3 \, M_\odot \, {\rm pc}^{-2}, \tag{12}$$

Including the stellar remnants, white dwarfs (Liebert, Dahn and Monet, 1988) and neutron stars, $\Sigma_{\rm wd+ns} = 2$ to 4 $M_\odot$ pc^{-2}, and an estimated interstellar gas contribution $\Sigma_{\rm gas} = 10$ to 15 $M_\odot$ pc^{-2} (Bahcall, 1984), the total surface mass density under the form of directly detected baryonic components in the disk is thus:

$$(\Sigma_\odot)_{\rm vis} = 40 \pm 4 \, M_\odot \, {\rm pc}^{-2} \tag{13}$$

in good agreement with Gould et al. (1997). The limits are derived from very conservative estimates for the errors. Using a sech$(|z|/z_0)^2$ vertical density distribution instead of an exponential profile leaves these values almost unchanged.

3.2. Bulge

The mass and the shape of the Galactic bulge will be discussed in more details in the next section. This mass is estimated to be $\sim 2 \times 10^{10} \, M_\odot$, from dynamical considerations (Zhao et al., 1996), with a size of about 1 kpc (Kent 1992). The faint end of the LF in the Baade's Window, down to $M_V \sim 10$, i.e. $m \approx 0.5 \, M_\odot$, has been studied with the HST Wide Field Camera (WFC) by Holtzman et al (1993). These authors find a Salpeter slope for the MF $x \approx 2.35 \pm 1$, over the afore-mentioned mass range. There is no indication for this MF to be different, except for its local normalization, from the one determined for the disk, Eq. (10).

3.3. Thick disk

A disk+bulge model does not reproduce successfully the observed star counts and kinematic properties. This led Gilmore & Reid (1983) to introduce the so-called *thick disk*, with a scale height $h_{\rm td} \approx 1 - 1.5$ kpc, which seems to be necessary for an accurate galactic modelling. Since the stellar velocity dispersion $\langle v_z^2 \rangle$ and the oblateness of the disk are related, a *thick* disk, by definition, is less elongated than the young (thin) disk, and has a larger velocity dispersion. This yields a better agreement with observed velocity dispersions, and with star counts in general. As shown recently by Reid et al. (1996) and Chabrier & Méra (1997), a thick disk with $h_{\rm td} \approx 1$ kpc and $q \approx 0.6$ is consistent with the Hubble Deep Field counts at faint magnitudes. A larger scale height and a spherically symmetric distribution predict substantially larger star counts. In spite of the small volume density of the thick disk in the solar neighborhood, about a few percents of the young disk at 1 kpc (Gilmore, Wyse & Kuijken; 1989), its contribution to the dynamics is not negligible since its surface density $\Sigma_{\rm td}(R) = \int_{-\infty}^{+\infty} \rho_{\rm td}(R,z)dz$ represents $\sim$ 10-20% of the young disk contribution.

Taking into account the thick disk contribution, and using the parameters derived by Gould et al. (1997), the disk stellar surface density is raised by $\sim 3 \, M_\odot$ pc^{-2} to

$$\Sigma_\star = 27 \pm 4 \, M_\odot \, {\rm pc}^{-2}, \tag{14}$$

so that the detected surface density (13) reads:

$$(\Sigma_\odot)_{\rm vis} = 43 \pm 5 M_\odot \, {\rm pc}^{-2} \tag{15}$$

3.4. Spheroid

The spheroid is also called in the literature the *stellar* halo. It is defined by a spherical density distribution decreasing as $\rho(r) \propto r^{-3}$ (Hubble profile) or equivalently a $r^{1/4}$, de Vaucouleurs profile. It differs from the central bulge essentially by a lower metallicity, $[M/H] \approx -1.5$ (Monet et al., 1992; Leggett, 1992; Baraffe et al., 1995, 1997) and larger velocity dispersions, $\sigma_R \approx 160$ km.s^{-1}, $\sigma_z = \sigma_\theta \approx 90$ km.s^{-1} (Dahn et al. 1995; Beers & Sommer-Larsen, 1995). The mass of the spheroid is $\sim 10^9 \, M_\odot$ (Bahcall, 1986) so its contribution to the galactic *mass* is not important. Its main contribution concerns the halo *star counts*.

Richer and Fahlman (1992) obtained for the spheroid a steeply rising LF down to the end of the observations whereas Dahn et al. (1995), from observations of high-velocity ($v_{\rm tan} > 200$ km.s^{-1}) subdwarfs in the solar neighorhood, get a LF which decreases at the faint end ($M_V \gtrsim 12$).

Méra, Chabrier & Schaeffer (1996) and Chabrier & Méra (1997) (see also Graff & Freese, 1996) have determined the MF of the spheroid from these observed LFs and from mass-magnitude relationships derived from LMS models which reproduce accurately the main sequences of metal-poor globular clusters, observed with the HST deep photometry surveys, down to the vicinity of the hydrogen burning limit (Baraffe et al., 1997). The spheroid MF in the solar neighborhood deduced from the Dahn et al. (1995) subdwarf LF is reasonably well parametrized as (Chabrier & Méra, 1997):

$$\mu(m) = 4.0 \pm 1.0 \, 10^{-3} \left(\frac{m}{0.1 \, M_\odot} \right)^{-1.7 \pm 0.2} M_\odot^{-1} \, {\rm pc}^{-3}, \tag{16}$$

Integration of this MF gives the halo main sequence ($m \leq 0.8\,\mathrm{M}_\odot$ for $t \geq 10$ Gyr) stellar density in the solar neighborhood:

$$\rho_{h_\star} \approx 1.0 \times 10^{-4}\,\mathrm{M}_\odot\,\mathrm{pc}^{-3} \qquad (17)$$

As shown by Chabrier & Méra (1997), star count predictions based on this MF are in excellent agreement with the Hubble Deep Field observations at very faint magnitudes both in the V and I-bands. Comparison of this value with the disk main-sequence stellar density determined in §3.1 gives the normalization of the spheroid/disk stellar population at 0.1 $\mathrm{M}_\odot$, namely $\rho_{\star_{sph}}/\rho_{\star_d} \sim 1/400$ (Chabrier & Méra, 1997).

3.5. Dark halo

Throughout this paper, the term "dark halo" defines what is characterized by the $\rho(r) \propto r^{-2}$ density-profile, a consequence of the flat rotation curve in the outer part of the Galaxy (see §2). The existence of a halo in the Galactic structure is rendered necessary i) to account for the total mass of the Galaxy (see §2.1.2), since the disk(s), bulge and spheroid total mass amounts at most to $\sim 10^{11}\,\mathrm{M}_\odot$ and ii) for stability conditions (Ostriker and Peebles, 1973), although the presence of a central bar weakens this latter argument. There is observational evidence that galactic dark halos present some oblateness with $q \sim 0.6$ (Sackett et al. 1994). Were the mass-distribution of the dark halo 2-dimensional (i.e. under the form of a disk), the surface density in the solar neighborhood, $\Sigma_\odot \approx v_{\mathrm{rot}}/2\pi G R_\odot = 210\,\mathrm{M}_\odot\,\mathrm{pc}^{-2}$ would be a factor 3 larger than the dynamical upper limit (see §2.2) (see Méra et al., 1997, Paper II). This condition, and the motion of galaxies and gas in the Local Group (§2.1) are strong arguments in favor of a large, 3-dimensional halo around the centre of the Galaxy.

The MF in the halo is presently unknown. The observation of the bottom of the stellar main sequence, $m \sim 0.1\,\mathrm{M}_\odot$, at a distance of 20 kpc, about the limit of the spheroid, requires surveys down to apparent magnitudes $I \gtrsim 28$ (Baraffe et al. 1997). It requires also an excellent angular resolution (< 0.1 arcsec) to distinguish stars from galaxies. This is the reason why early attempts using ground-based observations were never brought to a conclusive end. The recent Hubble Deep Field star counts (Flynn et al., 1996; Reid et al., 1996; Mendez et al., 1996) up to $I = 28$ are insufficient to determine a halo LF, because of the limited field of view, but represent a severe constraint on the Galactic model. These faint magnitude star counts have been shown to be entirely consistent with a thick disk + flattened spheroid population, characterized by their respective I-(V-I) relationships and mass functions (10) and (16) (Chabrier & Méra, 1997). As shown by these authors, a (even flattened) dark halo with the afore-mentioned $1/r^2$ profile and MF(16) would predict at least 500 more stars than observed in the HDF field of view. This shows that, if the dark halo LF is the same as the spheroid one, there is a negligible stellar population in the *dark halo*, less than 0.1% of the dynamical mass.

A promising technique to determine more accurately the halo MF comes from the recent surveys of the outer parts of nearby galaxies (Sackett et al. 1994; Lequeux et al. 1996) and

from the relation between the slope of the MF and the inferred colors of the halo diffuse emission (Méra, 1997).

Another important indication is given by the LFs of globular clusters. The MFs of the different clusters observed with the HST have been determined recently by Chabrier & Méra (1997). The typical LFs, determined near the respective half-mass radii, are rising up to $M_{\mathrm{bol}} \sim 10$ and drop below. This is consistent with monotonically *rising* MFs down to $\sim 0.1\,\mathrm{M}_\odot$, with a very weak dependence on metallicity, well described by power-law functions with $\alpha \sim 0.5 - 1.5$, similar to the ones determined in the previous sections for the disk and the spheroid. Although mass segregation effects are expected to be small near the half-mass radius (see e.g. King et al., 1995; Chabrier & Méra, 1997), the evolution of the clusters, and their evaporation, might lead to *initial* MFs (IMF) slightly steeper that the afore-mentioned determination. This would yield even better agreement with the MF (16) and would be consistent with the suggestion that the formation of spheroid field stars and globular clusters has occured in a similar manner and time frame (Fall and Rees, 1985).

Since the dark-halo stellar population is likely to be insignificant, as mentioned above, Eq. (16) gives the total halo (spheroid + dark halo) stellar contribution to the dynamically-determined local density $\rho_{\mathrm{dyn}} \sim 0.01\,\mathrm{M}_\odot.pc^{-3}$, namely $\rho_{h_\star}/\rho_{\mathrm{dyn}} \sim 1\%$. This puts more stringent limits than the ones obtained from the HST counts alone (Flynn et al., 1996) and shows convincingly that low-mass stars represent a completely negligible fraction of the halo mass.

In summary, the star count analysis of different stellar populations corresponding to different regions of the Galaxy, based on accurate evolutionary models for low-mass stars (Baraffe et al., 1997; Chabrier et al., 1996, 1997), leads to the determination, slope and normalization, of the MF in the disk, the bulge and the spheroid, down to the bottom of the main sequence. Surprisingly enough, given the different metallicities in these regions and the wide range of stellar masses considered, these MF's are very similar and reasonably well described by power-law MFs $dN/dm \propto m^{-\alpha}$ with $\alpha \approx 1.5-2$. A flatter MF below $\sim 0.5\,\mathrm{M}_\odot$ for the disk, as suggested by the HST LF, cannot be excluded but a more precise determination requires better statistics at the faint end of the LF. These MFs, consistent with all observed LFs and deep-photometry counts, yield a fairly well determined contribution of *all main sequence stars* to the disk and halo *mass budgets*, the dark halo stellar contribution to the Galactic mass being essentially insignificant. The determination of the amount of mass under the form of *sub-stellar* objects requires the analysis of the microlensing experiments.

4. Microlensing

Within the past few years the microlensing technique has been applied succesfully to the search for dark matter, by inferring the presence of dark objects in the Galaxy through their gravitational effect on luminous matter, as proposed initially by Paczyński (1986). Several groups worldwide have carried out microlensing experiments to determine the amount of dark matter either in the halo of the Galaxy (EROS and MACHO experi-

ments) or in its central parts (OGLE and MACHO experiments). We examine below these various experiments and connect the results with the afore-mentioned stellar MFs to determine the contribution of *sub-stellar objects* to the galactic mass budget.

4.1. Disk and bulge

Numerous events have been detected in the direction of the Galactic centre by the OGLE (Paczyński et al., 1996) and MA-CHO (Alcock et al. 1997) surveys. We focus here on the 40 events[4] obtained from the first-year analysis of the MACHO collaboration, whose detection efficiency $\epsilon(t)$ is well determined (Alcock et al., 1997). The number of events observed by OGLE during the first two years is too small and the attempt to use averages would be dominated by small number statistics. At any rate, adding, as an extreme value, the 9 OGLE events to the 40 MACHO ones would not improve significantly the statistics.

The interpretation of the three large-time events ($t_e > 75$ days) in the MACHO survey is still unclear and will be discussed below. Note that there is no event with $35 < t_e < 75$ days.

The number of observed events allows a statistical analysis from their time distribution. The average effective time $\langle t_e \rangle$ can be used to estimate the average lens mass $\langle m \rangle$ and thus the minimum mass down to which the mass function (10) extends (see Appendix):

$$\langle \sqrt{m} \rangle = \frac{c}{2\sqrt{GL}} \langle t_e \rangle \langle \frac{1}{v_\perp} \rangle^{-1} \langle \sqrt{x(1-x)} \rangle^{-1} \tag{18}$$

where the averages are relative to the effective probability distributions P_{eff} for each variable (see Appendix). For a simple gaussian velocity distribution, $\langle \frac{1}{v_\perp} \rangle^{-1} = \sigma\sqrt{\pi/2}$, where σ is the velocity dispersion. The geometric factor $\langle \sqrt{x(1-x)} \rangle$ is approximatly 0.39 for a standard (Bahcall & Soneira, 1980 + Kent, 1992) disk+bulge model, and is not very sensitive to the choice of the model. The mean duration of the 40 events, taking into account the experimental efficiency, is $\langle t_e \rangle = 16.8$ days (omiting the efficiency leads to $\langle t_e \rangle = 20$ days). Then a first estimate of the average lens mass is:

$$\langle \sqrt{m} \rangle^2 = 0.15\,\mathrm{M}_\odot \tag{19}$$

which is only a rough estimate, with a velocity dispersion $\sigma = 100\,\mathrm{km.s}^{-1}$ for the bulge. Excluding the three longest events yields $\langle \sqrt{m} \rangle^2 = 0.09\mathrm{M}_\odot$. These estimates introduce the dilemma that will be discussed in detail below: in the first case, microlensing results are compatible with essentially no brown dwarf in the disk/bulge, whereas in the second case, the mass function must extend significantly in the brown dwarf domain.

As mentioned in the Appendix A.2, we stress that $P(t_e)$ has a long power-law tail at large times, since $t_e \propto v_\perp^{-1}$, which yields an unphysical divergence of the moments. Therefore, the statistics for the mass of the microlensing events can *not* be evaluated correctly from the calculation of the moments, as done

sometimes in the literature, but must be evaluated accurately by using the detailed time distribution (Note, however, that the moments of $1/t_e$ behave correctly).

We have calculated the time distribution with a Monte-Carlo algorithm (see Appendix), which determines the number of events:

$$N_{th} = E \times \int_0^{+\infty} \epsilon(t_e) \frac{d\Gamma}{dt_e}\, dt_e \tag{20}$$

where E is the total exposure (in star-years) and ϵ the experimental efficiency factor (Alcock et al., 1997). Calculations have been done for a standard disk model (Bahcall & Soneira, 1980), and a Kent (1992) model for the bulge, for the two MFs considered in §3.1. We have taken velocity dispersions $\sigma \sim 100$ km.s^{-1} for the bulge and $\sigma \sim 20$ km.s^{-1} for the disk (40 km.s^{-1} in the radial direction), respectively, with a linear interpolation in the intermediate region located between ~ 2 and 3 kpc from the Galactic center. As will be shown below, the uncertainty in the velocity distribution of the stars is the main cause of uncertainty in the present calculations.

Our calculations take into account the motion of the Sun and of the source star in the determination of the lens velocity as well as the variation of the distance of the *source* stars in the disk and the bulge (see Appendix). The distance of the source stars in the bulge is typically 7.5 kpc from the Sun, as determined by Holtzman et al. (1993) from the observed LF in Baade's Window. The time-distribution and number of events obtained from these calculations, for a given model, are compared to the MACHO observations (Alcock et al., 1997). Since the efficiency does not include binary events, we must exclude those events. However, only a small fraction of the events are expected to be due to both components of a binary system (1 out of 45 in the first year, a fraction which seems to be confirmed by the following two years). In most cases, the Einstein disks of the stars in a multiple system do not overlap, and can in first approximation be treated independently. The time distribution is therefore barely affected by the binarity. Anyway the number of events has to be corrected only slightly (typically a few percent). In this section, we are mostly interested in the determination of the mass function in the substellar regime, which is derived only from the time distribution of the observed events. The consistency between models and observations is analyzed with a Kolmogorov-Smirnov (KS) test[5].

We will first assume that the mass function in the bulge is the same as in the solar neighborhood. The mass function is extrapolated in the brown dwarf domain down to a minimum mass, m_{inf}, which is determined when the best agreement between theory and observation is achieved. The results are shown in Fig. 2, for the mass functions (a) and (b) defined in §3.1, with

---

[4]　We have excluded the two events that fail MACHO cuts (104-B and 111-B), two events suspected to be variable stars (113-C and 121-B) and the binary event which is not accounted for by the efficiency.

[5]　The KS test does not give a confidence level, but rather an exclusion criterium. Its significance function has a very rapid variation between 10% (distributions most probably different) and 90% (distributions most probably identical), and any value in between does not give a strong conclusion. But the KS test is better than the χ^2 test for low statistics, and does not depend on any binning of the data.

$m_{inf} = 0.075\,M_\odot$ and $m_{inf} = 0.05\,M_\odot$, respectively. The KS test gives a probability of 85% for MF (a) and only 45% for MF (b). The value $m_{inf} = 0.05\,M_\odot$ for MF (b), and its steeper slope in the brown dwarf domain renders MF (b) very similar to a Dirac delta-function. Longer timescale events are then more difficult to reproduce. On the other hand, for MF (a), the relative contribution of higher masses is larger, with a better fit of the long timescale observations.

We have also computed the time distribution in case (b) with $m_{inf} = 0.1M_\odot$, which correspond to the absence of brown dwarfs in the disk. This corresponds to the general decreasing behaviour of the HST MF, ignoring the last bin. The time distribution, also shown in Fig. 2, is incompatible with the observed time distribution, with a KS result of 5%, as already pointed out by Han and Gould (1995). These results suggest that brown dwarfs are required to explain all the 40 events of the MACHO first year bulge observations, unless the effect of amplification bias (Alard, 1997; Han, 1997) is important enough to account for the excess of short timescale events.

It has been suggested (Alcock et al 1997; Han and Gould, 1995) that the large time events may have another origin than main sequence stars, and might be due to stellar remnants, white dwarfs or neutron stars. They may be due also to rare statistical fluctuations due to the large tail of the time distribution or, more speculatively, to dwarf nova eruptions (Della Valle and Livio, 1996). If we exclude the 3 longest events from the present analysis, the agreement between theory and observation improves significantly, as shown in Fig. 3 for the same MFs. This yields minimal masses for the two mass functions $m_{inf} = 0.056\,M_\odot$ in case (a), and $m_{inf} = 0.047\,M_\odot$ in case (b). The KS significance of the two MFs is 50% in case (a) and 40% in case (b).

The minimum masses given above depend on the model used for the calculations, in particular the poorly-determined velocity dispersions in the bulge population (Ibata & Gilmore, 1995). This yields the largest uncertainties in the present results, since $\langle m \rangle \propto \langle \sigma^2 \rangle$.

These mass functions yield a brown dwarf contribution to the surface density in the solar neighborhood, assuming the same scale height as for the M-dwarf population, i.e. $h_d \sim 300$ pc:

$$\Sigma_{bd} \approx 3 \pm 3\,M_\odot\,pc^{-2} \tag{21}$$

Therefore the brown dwarf contribution to the local surface density is about 10% to 20% of the total stellar contribution (14). This represents $\sim 10\%$ of the observed baryonic mass (15). As shown in Eq. (21), the brown dwarf contribution is also compatible with zero. The *total* surface density in the form of baryonic matter in the disk is thus (Eqs. (15) and (21)):

$$\Sigma_{baryon} = 46 \pm 6\,M_\odot\,pc^{-2} \tag{22}$$

consistent with the dynamical determination (8). There is no need for any additional dark matter. The contribution of *stellar and substellar objects* to the surface density is (Eq.(14) and Eq.(21)):

$$\Sigma_{ss} = 30 \pm 5\,M_\odot\,pc^{-2} \tag{23}$$
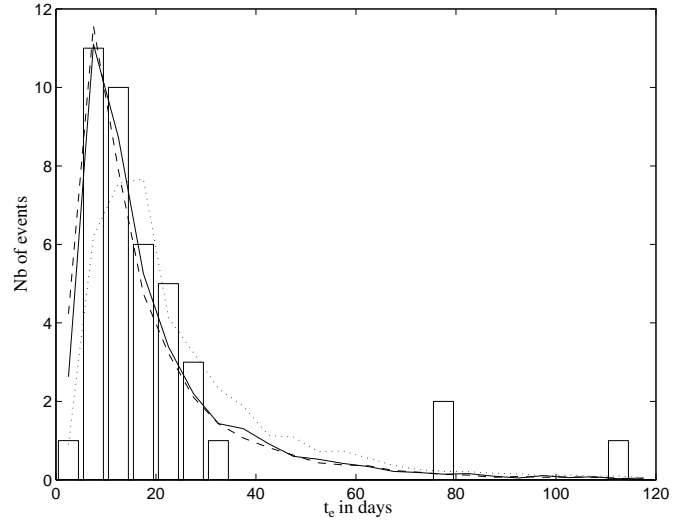
Fig. 2. Observed time distribution (histograms) for all MACHO events compared with the distribution of two models. Solid line: MF (a) with $m_{inf} = 0.075\,M_\odot$, dashed line: MF (b) with $m_{inf} = 0.05\,M_\odot$, and dotted line: MF (b) with $m_{inf} = 0.1\,M_\odot$. The latter case is excluded by a KS test (see text), showing that brown dwarfs are required to explain the observed distribution.
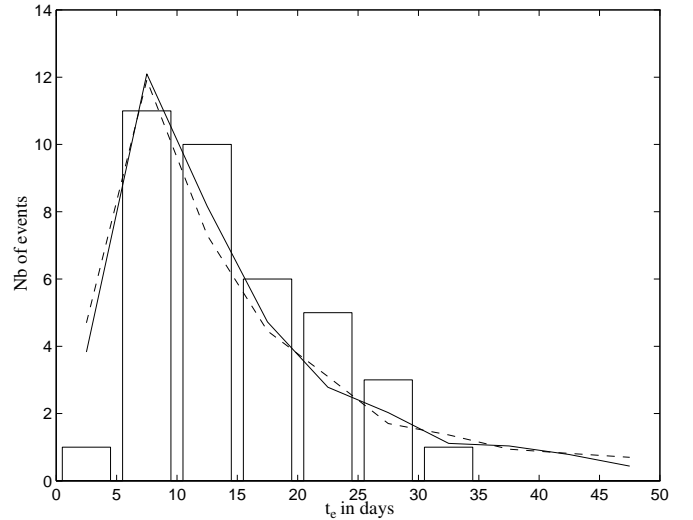
Fig. 3. Same as Fig. 2, without the three longest events (see text). Models are: MF (a) with $m_{inf} = 0.056\,M_\odot$ (solid line), MF (b) with $m_{inf} = 0.047\,M_\odot$ (dashed line).

This yields an optical depth (see e.g. Kiraga & Paczyński, 1994):

$$\begin{aligned}
\tau_{disk} &\approx \frac{2\pi G}{3c^2}\rho_* R_\odot^2 \\
&\approx 5.5 \times 10^{-7}\,\frac{\Sigma_{ss} + 50 M_\odot\,pc^{-2}}{50 M_\odot\,pc^{-2}} \\
&\approx 9.0 \pm 0.5 \times 10^{-7},
\end{aligned} \tag{24}$$

i.e. $\tau_{disk} \lesssim 10^{-6}$, a factor ~ 2 to 3 smaller than the observed value $\tau_{obs} \sim 2.4 \pm 0.5 \times 10^{-6}$ (Alcock et al., 1997). Therefore,

although the observed time-distribution of the events is well reproduced by the present model, the optical depth amounts to $\sim 1/3$ of the observed value. This clearly suggests a bulge strongly elongated along the line-of-sight or, similarly, a bar model (Zhao 1994). We have not included a bar-model in our calculations, but from the present analysis, its contribution to the optical depth corresponds to:

$$\tau_{\text{bar}} \approx 1 \times 10^{-6}\, M_{\text{bar}}/(10^{10} \text{M}_\odot) \tag{25}$$

in good agreement with various models (Zhao, Spergel & Rich, 1995, 1996; Han & Gould, 1995; Stanek et al., 1997; Bissantz et al., 1997). Infrared observations from DIRBE seem to constrain the mass of the bulge within 2.4 kpc to $M_b \sim 7.2-8.6 \times 10^9$ M$_\odot$, although this value is obtained by substracting a model-disk contribution; a more general constraint concerns the *bulge+disk* mass $M_{b+d}(< 2.4 \text{ kpc}) = 1.9 \times 10^{10}$ M$_\odot$ (Bissantz et al., 1996). Note however that the three long-time events contribute about 1/3 to the observed optical depth, so that the discrepancy between the value (24) and the observed one is reduced appreciably if these events are removed, leading to a smaller mass for the bulge. Moreover, as noted recently by Han (1997) and Alard (1997), the optical depth toward the bulge might be overestimated by as much as a factor 1.7, because of amplification bias due to pixel lensing.

4.1.1. Events whose source is a bulge clump giant

As mentioned by Alcock et al. (1997), there are significant uncertainties in the estimated bulge optical depth, because essentially of blending effects. For this reason, the MACHO collaboration has conducted a separate analysis of the events whose source is a bulge *giant* (Alcock et al. 1997). Although the statistics are significantly diminished (1.3×10^6 source giants and 13 events), the efficiency and the reliability of the results are improved appreciably. The corresponding optical depth is also substantially larger, but only at the $\sim 1\sigma$ level, than the value obtained when including the totality of the events, namely $\tau_{\text{giant}} \sim 3.9 \times 10^{-6}$. The mean duration of these events is $\langle t_e \rangle = 33.8$ days, which yields an unrealistic average mass of 0.6 M$_\odot$ from relation (18). This high value is confirmed by the complete calculation, with a minimum mass $m_{\text{inf}} \approx 0.3M_\odot$. This minimum mass is the same for both MFs (a) and (b) because they are identical for $m > 0.35$M$_\odot$. Such a high minimal mass is not allowed in the disk, since many stars with mass $m < 0.3$ M$_\odot$ are observed in the solar neighbor hood. Therefore, either the bulge mass function is different from the disk MF, or the three long time scale events have a different origin (most likely stellar remnants).

Without including the three afore-mentioned long-time events, which all correspond to a bulge clump giant source, the mean duration is $t_e = 16.7$ days, yielding an average mass of 0.15 M$_\odot$. The minimum mass derived with the complete calculations to reproduce the time distribution in that case is $m_{\text{inf}} = 0.11$ M$_\odot$ in case (a) and $m_{\text{inf}} = 0.07$ M$_\odot$ in case (b). The KS test gives a result of 70% in both cases. Fig. 4 shows the model distribution compared to observations in case (a). It

is thus possible to explain the observed time distribution with a main sequence stellar population with the mass function (a) or (b) plus a stellar remnant population.

4.1.2. Events whose source is a disk main sequence star

The OGLE collaboration (Pacziński et al., 1994) and the MACHO collaboration (Alcock et al., 1997), have observed the same region, near the Baade's window, in the direction of the bulge. The MACHO collaboration observed *six* events whose source lies on the *disk* MS, with a magnitude $V \lesssim 18.5$. The sources of 3 of these 6 events lie near the very red edge of the MS and could well be bulge blue helium core burning giants. This could be easily verified from their spectra. However, the remaining 3 sources are likely to be disk MS stars. These events yield an optical depth 7.5×10^{-7}, whereas the standard disk model (with no dark population) yields $\sim 10^{-7}$ and a *maximal disk* (see Paper II) yields $\sim 2 \times 10^{-7}$. But the MACHO efficiency used for the derivation of this optical depth is an average over all source stars. Since we are considering only sources with $V < 18.5$, the efficiency for these brighter sources must be higher. With an extreme (unlikely) 100% efficiency, the optical depth for disk sources is $\tau = 2 \times 10^{-7}$ in better agreement with disk models. We stress that theoretical estimates depend strongly on the disk scale length and scale height.

The average time for the corresponding 3 events is $\langle t_e \rangle = 4.4$ days. Since the source stars are as bright as the bulge clump giants, the blending is expected to be negligible for these events. The mean duration would correspond to a minimum mass smaller than 0.005 M$_\odot$, definitely in the brown dwarf domain. However, the extrapolation of either mass function (a) or (b) down to a minimum mass of 0.005 M$_\odot$ requires a moderate power-law exponent in order not to exceed the local dynamical limit ($\Sigma_{\text{bd}} = 27$ M$_\odot$ pc^{-2} if $\alpha = 2$ and $\Sigma_{\text{bd}} = 62$ M$_\odot$ pc^{-2} if $\alpha = 2.5$ for MF (a)). Moreover, such a low minimum mass overproduces short time scale events for bulge sources, especially when only clump giant sources are considered.

Fig. 4 shows the calculated time distribution of the microlensing events obtained with the MF (a) with *two different minimum masses* for the bulge and the disk, as inferred from §4.1.1 and 4.1.2. A minimum mass $m_{\text{inf}} = 0.3$ M$_\odot$ for the *bulge* and $m_{\text{inf}} = 0.015$ M$_\odot$ for the *disk*, with both MFs (a) and (b). The model distributions agree with a 70% KS result with the observed one. Such a disk brown dwarf population corresponds to a local surface density:

$$\Sigma_{\text{bd}} \approx 20 - 30 \, \text{M}_\odot \, \text{pc}^{-2} \tag{26}$$

Clearly any solution between the above one and the one where $m_{\text{inf}} \sim 0.1$ M$_\odot$ everywhere (cf §4.1.1), i.e. no brown dwarf, looks acceptable. The disk contribution to the bulge optical depth in this model is $\tau_d \approx 8 \times 10^{-7}$, slightly larger than the optical depth of a standard (no brown dwarf) disk (5×10^{-7}), but still insufficient to explain the observed $\tau \approx 4 \times 10^{-6}$.

Whereas small number statistics and uncertainty in the distance of the sources prevent a reliable determination of the brown dwarf contribution to the disk mass budget in this case,
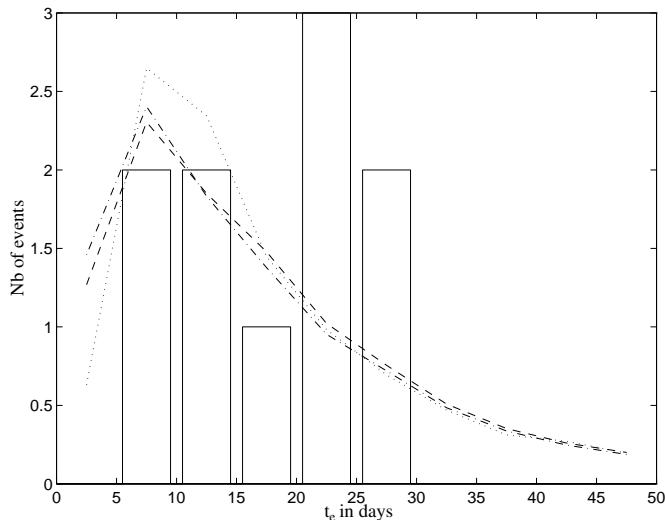
Fig. 4. Comparison of the giant bulge events (excluding the 3 longest events) with three models. Dotted line: the MF (a) is assumed to be the same for both the bulge and the disk, with $m_{inf} = 0.11\,M_\odot$. Dashed line: the disk MF has a $m_{inf} = 0.015\,M_\odot$ and the bulge MF has a $m_{inf} = 0.4\,M_\odot$, for MF (a); the dot-dashed line is the same for MF (b). The histogram corresponds to observations.

the present analysis corresponds to a brown dwarf and a dynamical density in the disk, from (15), (21) and (26):

$$\Sigma_{bd} \approx 0 - 30\,M_\odot\,pc^{-2} \quad ; \quad \Sigma_\odot \approx 40 - 70\,M_\odot\,pc^{-2}, \quad (27)$$

possibly larger than the value (8) determined in §2.1. A mass-dependent scale height does not change significantly the brown dwarf contribution, unless their scale height is larger than ~ 1 kpc.

These results leave open the following possibility: **i)** the mass functions of the disk and the bulge are different, in particular in term of minimum mass, and **ii)** the dynamical upper limit for $\Sigma_\odot$ (Eq. 8) and the observed density of baryonic matter (Eq. 15) imply that 20 to 30 $M_\odot\,pc^{-2}$ of the solar surface density can be in the form of brown dwarfs, in agreement with the microlensing analysis (Eq. 27). Note that the possibility for the disk and bulge mass functions to be different has also been suggested by Gould et al. (1997) to reconcile star counts and microlensing observations. However, although these authors invoke a large population of brown dwarfs in the *bulge*, the present analysis suggest that they could as well be located in the *disk*. A more precise determination of the amount of brown dwarfs in the disk requires microlensing observations optimized for characteristic timescales of a few days, corresponding to a sampling of two observations per day. We stress the need for such microlensing searches.

The present analysis illustrates the difficulty to reach robust conclusions about the mass under the form of sub-stellar objects in the central regions of the Galaxy, and more precisely in the disk and the bulge, from present microlensing experiments. The situation will certainly be clarified once future projects will be operational, allowing much better statistics in both parts of the

Galaxy. In fact, the MACHO survey has now a total of more than 200 candidate microlensing events, still under analysis, which will improve the present determinations.

The volume density of *disk* brown dwarfs in the solar neighborhood deduced from the two types of calculations described above, global vs separate disk/bulge analysis, correspond respectively to $\rho_{BD} \sim 5 \times 10^{-3}\,M_\odot\,pc^{-3}$ (from Eq. 21) within about a factor 2, and $\rho_{BD} \sim 3 - 5 \times 10^{-2}\,M_\odot\,pc^{-3}$ (from 3 events in the disk, Eq. (26): this is clearly to be revised in the light of future observations), a factor 10 more. Future deep photometry and large field observational surveys might thus help determining the present issue by direct observation of nearby brown dwarfs, although the small density and the intrinsic faintness of brown dwarfs ($M_V \gtrsim 22$, Baraffe et al. 1997) renders the observation of a statistically-significant sample of field brown dwarfs a tremendously difficult task. Note that infrared filters are highly recommended for these objects ($M_J \gtrsim 12$; $M_K \gtrsim 11$, Baraffe et al. 1997).

The present analysis is thus an indication that an important amount of brown dwarfs in the disk is not excluded with present day observations, as suggested by the rise of the disk mass function near $0.1M_\odot$ (cf. §3.1).

4.2. Spheroid

For a DeVaucouleurs spheroid, extrapolation of the MF (16) into the brown dwarf region, even with $m_{inf} = 0.01\,M_\odot$, yields a number of microlensing events towards the LMC of ~ 0.4 and an optical depth $\tau_{sph} \sim 5 \times 10^{-9}$ (Chabrier & Méra, 1997). This illustrates the negligible contribution of the spheroid to the Galactic mass, and thus to the events observed towards the LMC.

4.3. Dark halo

The analysis of the *first year* of the EROS (Aubourg et al., 1993) and MACHO (Alcock et al., 1993) microlensing observations towards the LMC had shown that the observed events were likely to be due to halo brown dwarfs, with an average mass $\langle m \rangle \approx 0.03\,M_\odot$ (Méra et al. 1996b; Kerins 1995). The inferred contribution of these objects to the missing mass was found to be between 10 and 20% (Alcock et al. 1995; Gates et al., 1995; Méra et al. 1996b). These calculations must now be re-examined in the context of the *second year* of the MACHO experiment.

These results yield now a total of 1 to 2 events observed by EROS (Ansari et al., 1996; Renault et al., 1997) and 6 to 8 by MACHO (Alcock et al., 1996). The inferred optical depth is much larger than derived previously, $\tau_{obs} = 2.2 \pm 1 \times 10^{-7}$, about 40% of the value corresponding to the standard halo. The 6 MACHO events[6] yield $\langle t_e \rangle \approx 40$ days, in reasonable agreement with the value inferred from the 2 events observed by EROS, $\langle t_e \rangle \approx 28$ days. The statistics, however, are not sufficient to

---

[6]   We have excluded the MACHO events #10, believed to be a variable star (Alcock et al., 1996), and #9, the binary event, which probably belongs to the LMC.

constrain a mass function from the time distribution. As will be shown in Paper II, the number of observed events cannot be explained by dark objects in the LMC itself. As shown by Chabrier & Méra (1997) and Graff & Freese (1996), extrapolation of the MF (16) into the brown dwarf domain yields a negligible fraction of brown dwarfs in the Galactic halo.

A substantial amount of these objects in the halo thus implies a significantly different, much steeper MF beyond the hydrogen-burning limit. In order to estimate the *maximum contribution* of halo substellar objects to the microlensing counts, we consider, as in Méra et al (1996b), a halo MF $\frac{dN}{dm}(m) \propto m^{-x}$ with $x = 5$, essentially a Dirac-peaked MF. The *maximum normalization* of $\frac{dN}{dm}(m)$ at 0.1 M$_\odot$ is the observed count of halo subdwarfs in the solar neighborhood, derived in §3.4. We thus take as the *upper limit* for the dark halo substellar mass function:

$$\frac{dN}{dm}(m) = 4.0 \times 10^{-3} \left(\frac{m}{0.1M_\odot}\right)^{-5} M_\odot^{-1} pc^{-3} \qquad (28)$$

A Kolmogorov-Smirnov test done on the t_e distribution of the EROS + MACHO halo events shows unambigously that such a MF is not consistent with the observations, whatever the value of m_{inf}. The optical depth can be reproduced only if $m_{inf} < 0.02M_\odot$, but the time distribution is in severe conflict with the observed one, as shown by a 0.02% KS probability ($\langle t_e \rangle$ = 12 days).

The expected average mass of microlensing events is related to the characteristic timescale of the event and to the velocity dispersion (see Appendix Eqs. A2 and A15). The average tangential velocity is proportional to the dispersion of the Gaussian velocity distribution $\langle 1/v_\perp \rangle^{-1} \propto \sigma$ (see Appendix). Assuming a *maximal* dark halo $\rho_h(r) = \rho_{dyn}/r^2$, where $\rho_{dyn} = 8 \times 10^{-3}$ M$_\odot$ pc^{-3} is the local dark matter density (Bahcall 1986), this dispersion corresponds to the asymptotic rotation velocity with the relation $\sigma = v_{rot}/\sqrt{2} \approx 150$ km.s^{-1}, where $v_{rot} \approx 220$ km.s^{-1}, as given by the isothermal sphere model (Binney and Tremaine 1987). This yields an average mass, corrected for blending, $\langle \sqrt{m} \rangle^2 \approx 0.4 - 0.5$ M$_\odot$, as suggested by the MACHO collaboration (Alcock et al., 1996). Several observations (Beers & Sommer-Larsen, 1995; Dahn et al., 1995; Layden et al., 1996) suggest that the halo population velocity ellipsoid is radially elongated, by a factor $\sim 1.5 - 2$. This yields a projection effect which decreases the velocity dispersion. On the other hand, this dispersion is bound by the velocity of the line-of-sight toward the LMC (Eq. A19), which is (after proper calculations), $\langle 1/v_{los} \rangle^{-1} \sim 80$ km.s^{-1}. This corresponds to a minimum mass $m_{inf} = 0.04$ M$_\odot$ but to a *zero* dispersion velocity, clearly an irrealistic possibility. When considering such a "modified" halo model, with a non-isotropic velocity dispersion tensor at 1σ of 80 km.s^{-1} and an important oblateness, the time distribution can be reproduced with $m_{inf} \sim 0.1M_\odot$, still above the hydrogen-burning limit. However, the number of observed events implies a normalization for the halo MF at 0.1 M$_\odot$ significantly larger than the maximum value (16), inferred from observed low-mass stars in the solar neighborhood.

These calculations show that, if the results of the recent MACHO analysis are confirmed, the possibility for halo dark objects to be field brown dwarfs is clearly excluded, even for a MF substantially steeper than the ones in the disk and the spheroid, for any halo model. This analysis, consistent with the MACHO observations (Alcock et al., 1996) and with star count analysis at faint magnitudes (Chabrier & Méra, 1997), and the one conducted in §3.4 and 3.5, suggest a negligible mass-fraction under the form of field stars and brown dwarfs in the dark halo. Different solutions to try to reconcile star counts and microlensing observations in the halo will be considered in Paper II.

5. Summary and conclusions

In this paper, we have examined in detail all the observational sources that constrain the mass distribution of the Galaxy. This includes dynamical constraints, circular rotation velocity and vertical velocity dispersion in the solar neighborhood, star counts in the disk, bulge and spheroid, and microlensing observations towards the Galactic halo and the Galactic center. The star counts yield the derivation of stellar mass functions for the disk, the bulge and the spheroid down to the bottom of the main sequence. A substantial discrepancy, however, remains between the MF inferred from the nearby LF and the one deduced from the HST LF in the range $0.09 - 0.35$ M$_\odot$. Although the nearby MF is consistent with a steadilly rising power-law $dN/dm \propto m^{-\alpha}$ with $\alpha \sim 2$ down to the bottom of the main sequence, the HST MF is essentially flat below 0.6 M$_\odot$. Interestingly enough, the significantly rising last bin of the HST MF, indicates an upturn of the MF near the brown dwarf domain, so that both type of MFs, nearby and photometric, suggest the presence of a substantial amount of brown dwarfs in the Galactic disk.

We have determined the normalization of these mass functions and shown that the ratio of the halo to disk main sequence stellar density is about $\sim 1/400$ near the bottom of the main sequence. The presence of the spheroid is proven unambiguously by the observed star counts of high velocity stars but its contribution to the Galactic mass is negligible. These calculations yield the determination of the contribution of main sequence stars, and thus of *observed* baryonic matter, to the disk and halo mass budget. The detected (thin+thick) disk stellar surface density corresponds to $\Sigma_{vis} \approx 43 \pm 5$ M$_\odot$ pc^{-2}, whereas the halo (spheroid + dark halo) density corresponds to less than $\sim 1\%$ of the dynamically determined dark matter, significantly less than the limit determined by the HST (Flynn et al., 1996).

The contribution of sub-stellar objects to this mass depends on the lower limit down to which the mass functions can be extrapolated. This limit is fixed by the microlensing observations, in particular by the time distribution of the events. This combined analysis of star counts for the luminous part of the mass function, which yields the determination of the slope and normalization near the brown dwarf limit, and of microlensing experiments, which determines the minimum mass, yields a *consistent determination* of the dark matter under the form of star-like objects, low-mass stars and brown dwarfs, in different parts of the Galaxy. Although uncertainties due to either small

statistics or ill-constrained velocity dispersion and location of the sources in the bulge prevent for now a precise determination, the derived brown dwarf surface density in the solar neighborhood, for a scale height $h_z = 320$ pc (Gould et al., 1997), is likely to be in the range $\Sigma_{bd} = 0 - 30\,M_\odot.pc^{-2}$ so that the total local density in the disk is $\Sigma_{dyn} \sim 40-70\,M_\odot\,pc^{-2}$. As will be shown in Paper II (Méra et al., 1997), this is in agreement with various observational determinations. More statistics of microlensing events towards the bulge will allow a separate determination of the brown dwarf contribution in the bulge and in the disk. An attempt based on the analysis of the events whose source is a clump giant or a disk main sequence star, respectively, yield rather surprising results (hampered by present observational uncertainties): most brown dwarfs would be present in the disk, whereas the bulge would contain almost none of these objects. This stresses the need for further observations in this region.

For the halo, we show that brown dwarfs have a negligible contribution ($\lesssim 1\%$) to the halo mass. A steep ($\alpha \gtrsim 2$) mass function in the halo seems to be excluded both by the microlensing analysis and by the M-dwarf LF. Therefore, the present analysis excludes main sequence stars and brown dwarfs as a significant contribution to the halo mass budget.

The nature of the dark events observed in the halo remains a puzzle. Halo white dwarfs remain the least unlikely candidates, although this scenario implies severe constraints on the age of the halo and its initial mass function (Chabrier et al., 1996; Adams & Laughlin, 1996). More attention will be devoted to this problem in Paper II.

These calculations, which combine observational constraints arising from star counts, microlensing experiments and kinematic properties, yield the consistent determination of the amount of dark matter under the form of stellar and sub-stellar objects in the differents parts of the Galaxy. This yields new insight on the distribution of baryonic dark matter in the Galaxy and bears important consequences for the derivation of a consistent Galactic mass-model. This will be examined in the next paper (Méra, Chabrier and Schaeffer, 1997, Paper II).

Appendix A: microlensing equations

The basic microlensing equations can be found for instance in Griest (1991) or in Kiraga and Paczyński (1994). However, we use some extra formulae which are given below, after a summary of the basic equations.

The duration t of a microlensing event is defined as the time during which the amplification of the monitored star is larger than a given threshold amplification A_T[7] (usually $A_T = 1.34$). The event duration corresponds to the crossing time of the Einstein disk, of radius $u_T R_e$, for the lens:

$$t = \frac{2R_e}{v_\perp}\sqrt{u_T^2 - u_{min}^2} = 53\text{ days }\frac{220\text{km.s}^{-1}}{v_\perp}\times$$

---

[7]   or equivalentely, a threshold impact parameter u_T in units of the Einstein radius, related to A_T by $A_T = \dfrac{u_T^2 + 2}{u_T\sqrt{u_T^2 + 4}}$.

$$\sqrt{\frac{m}{0.1M_\odot}}\sqrt{\frac{L}{55\text{ kpc}}}\frac{\sqrt{x(1-x)}}{0.5}\sqrt{u_T^2 - u_{min}^2} \qquad (A1)$$

where $v_\perp$ is the lens transverse velocity w.r.t. the line of sight, u_T (resp. u_{min}) is the impact parameter corresponding to the threshold amplification (resp. maximum amplification) A_T, L is the distance to the source, xL and m denote respectively the distance and the mass of the lens, and $R_E = \frac{2}{c}\sqrt{GmLx(1-x)}$ is the Einstein radius.

The *characteristic* time of an event is defined as:

$$t_e = \frac{R_e}{v_\perp} = \frac{2}{cv_\perp}\sqrt{GLmx(1-x)} = \frac{t}{2\sqrt{u_T^2 - u_{min}^2}} \qquad (A2)$$

This effective time does not depend on the impact parameter, and can be recovered from the observations with the relation between u_{min} and the known maximal amplification. In practice, the blending (several unresolved stars of which only one is amplified) renders this process rather difficult. The overall effect of blending is to underestimate the characteristic time.

The probability for a source star to be microlensed at a given time is called the optical depth, and reads:

$$\tau = \int_0^1 u_T^2 \pi R_e^2 \frac{\rho(xL)}{m}L\,\mathrm{d}x =$$

$$\int_0^1 u_T^2 \pi \frac{4GL^2}{c^2}\rho(xL)x(1-x)\,\mathrm{d}x \qquad (A3)$$

where $\rho(xL) = \int_0^\infty \rho_m(xL)dm$ is the total mass-density under the form of dark objects.

The experimental optical depth is retrieved from observations by:

$$\tau_{exp} = \frac{\sum t_{obs}/\epsilon(t)}{N_s \times T_{obs}} \qquad (A4)$$

where N_s and T_{obs} denote the number of source stars and the total duration of the experiment, respectively whereas $\epsilon(t)$ is the detection efficiency.

A.1. Event rate

The theoretical event rate for a given Galactic model, i.e. the expected number of events per unit time, reads:

$$\mathrm{d}\Gamma = 2u_T R_e v_\perp \frac{\rho(xL)}{m}\mathrm{P}(m)\mathrm{P}(v_\perp)\,\mathrm{d}m\,\mathrm{d}v_\perp\,\mathrm{d}x \qquad (A5)$$

where $\mathrm{P}(m)$ and $\mathrm{P}(v_\perp)$ are the probability distributions respectively of lens mass and velocity. If the velocity distribution is independent of the position, the integration of (A5) yields:

$$\Gamma = u_T \frac{4}{c}\sqrt{GL}\int_{m_{inf}}^{m_{sup}}\frac{1}{\sqrt{m}}\mathrm{P}(m)\,\mathrm{d}m$$

$$\times \int_0^L \sqrt{x(1-x)}\rho(xL)\mathrm{d}(xL)\int_0^{+\infty}\mathrm{d}v_\perp v_\perp\mathrm{P}(v_\perp) \qquad (A6)$$

For N_s source stars monitored during T_{obs}, the expected *number* of events is:

$$N = \Gamma \times N_s T_{obs} \tag{A7}$$

The relation (A5) shows that the *effective* microlensing probability distributions are different from the model distributions, and are given by:

$$P_{eff}(x) \propto \sqrt{x(1-x)}\rho(xL) \tag{A8}$$

$$P_{eff}(v_\perp) \propto v_\perp P(v_\perp) \tag{A9}$$

$$P_{eff}(m) \propto \frac{P(m)}{\sqrt{m}} \tag{A10}$$

For a Maxwellian velocity distribution, of dispersion σ, the transverse velocity reads:

$$P(v)\,dv = \frac{1}{2\pi\sigma^2}e^{-\frac{v_x^2+v_y^2}{2\sigma^2}}\,dv_x\,dv_y = \frac{v}{\sigma^2}e^{-\frac{v^2}{2\sigma^2}}\,dv \tag{A11}$$

and

$$P_{eff}(v) = \frac{vP(v)}{\int_0^{+\infty} v'P(v')\,dv'} = \sqrt{\frac{2}{\pi}}\frac{v^2}{\sigma^3}e^{-\frac{v^2}{2\sigma^2}} \tag{A12}$$

which yields:

$$P(t_e) =$$

$$\frac{\int \frac{P(m)}{\sqrt{m}}\sqrt{x(1-x)}\rho(xL)\sqrt{\frac{2}{\pi}}\frac{R_e^2}{t_e^2\sigma^3}e^{-\frac{R_e^2}{2\sigma^2 t_e^2}}\frac{R_e}{t_e^2}\,dx\,dm}{\int \frac{P(m)}{\sqrt{m}}\sqrt{x(1-x)}\rho(xL)\,dm\,dx} \tag{A13}$$

and (with use of Eq. (A6)):

$$P(t_e) = \frac{32G^2L^3u_T}{c^4t_e^4\Gamma\sigma^2}$$

$$\times \int mP(m)\left[x(1-x)\right]^2\rho(xL)e^{-\frac{2GLmx(1-x)}{c^2\sigma^2 t_e^2}}\,dx\,dm \tag{A14}$$

For a given Galactic model, we use a Monte-Carlo algorithm to calculate the event rate, which yields a set of simulated events whose time distribution is exactly the one given by (A14).

These equations yield the average characteristic time $\langle t_e\rangle$:

$$\langle t_e\rangle = \frac{2\sqrt{GL}}{c}\langle\sqrt{m}\rangle\langle\frac{1}{v_\perp}\rangle\langle\sqrt{x(1-x)}\rangle \tag{A15}$$

In Eq. (A15), the means are computed with the effective probability distributions (A8-A10). When writing explicitly the corresponding integrals, we can identify the optical depth and the event rate, which yields:

$$\tau = \Gamma \times \frac{\pi}{2}u_T\langle t_e\rangle. \tag{A16}$$

A given Galactic model implies a time-distribution $d\Gamma/dt_e = \Gamma \times P(t_e)$ and the number of events predicted by the theory is given by:

$$N_{th} = E \times \int_0^{+\infty} \epsilon(t_e)\frac{d\Gamma}{dt_e}dt_e \tag{A17}$$

where $E = N_s \times T_{obs}$.

A.2. Divergence of the moments

As shown in Eq. A13, the probability to observe an effective time t_e behaves as:

$$P(t_e)dt_e \propto 1/t_e\,P(v_\perp)dv_\perp \propto v_\perp^3\,dv_\perp \tag{A18}$$

so that $P(t_e)$ has a long power-law tail at large times. This yields the divergence of the moments of order $n > 3$ $\int t_e^n P(t_e)dt_e$, which causes the extreme sensitivity of $\langle t_e\rangle$ and τ to the rare large-time events. This long-range tail effect, which prevents the use of the higher order moments of t_e, is also felt when the central limit theorem is invoked to identify the *observed* average time of e.g. the 45 events with the *statistical* average. They are equal in the large-N limit, but the convergence is extremely slow in this case. This shortcoming is fixed by using the average $\langle\frac{1}{t_e}\rangle$ instead of $\langle t_e\rangle$. This method is more useful to constrain m_{inf} and $\langle t_e\rangle$ than Eq .A15 since $1/t_e \propto v_\perp$ and is thus nearly gaussian at the beginning and $1/t_e \propto m^{-1/2}$ and is thus most sensitive to the low mass end of the mass function.

A.3. Motion of the line of sight

The lens velocity w.r.t. the line-of-sight (l.o.s.) depends on the motion of the l.o.s. itself and must include the motion of the Sun and of the source star w.r.t. the Galactic center. The lens velocity thus reads:

$$\boldsymbol{v} = \boldsymbol{v}_{lent.} - x\boldsymbol{v}_{source} - (1-x)\boldsymbol{v}_\odot \tag{A19}$$

The velocity now depends on the lens distance xL, and Eqs. (A11-A14) relative to a gaussian velocity distribution, are no longer valid. Straightforward calculations yield the projected velocity of the lens w.r.t. the l.o.s.:

$$v = \left[\left(v_{lent.,l} - v_{\odot,l} + x(v_{\odot,l} - v_{s,l})\right)^2\right.$$

$$\left.+ \left(v_{lent.,b} - v_{\odot,b} + x(v_{\odot,b} - v_{s,b})\right)^2\right]^{1/2} \tag{A20}$$

A.4. Distance of the source star

In the case of the bulge, the elongation along the line of sight is no longer negligible, and the afore-mentioned formulae must include the possible variation of the distance L of the source, which implies an extra integral on L:

$$\tau = \frac{\int_0^{+\infty} L^2\nu_s(L)\,dL\int_0^1 u_T^2\pi\frac{4GL^2}{c^2}\rho(xL)\sqrt{x(1-x)}\,dx}{\int_0^{+\infty} L^2\nu_s(L)\,dL} \tag{A21}$$

where ν_s is the density of source stars *visible* at the distance L. This requires a luminosity function for the source stars. Following Kiraga and Paczyński (1994), $\nu_s \propto \rho L^{2\beta}$, if the number of stars brighter than some absolute luminosity L is proportional to L^β. We have slightly modified ν_s to take into account the fact that giant stars have more or less the same luminosity. Then $\nu_s \propto \rho(L^{2\beta}+C)$ where C is adjusted to reproduce the observed ratio of giants.

The event rate (A6) now reads:

$$\Gamma = \frac{4\sqrt{G}}{c \int_0^{+\infty} \nu_s(L)L^2 \, \mathrm{d}L} \int_0^{+\infty} \mathrm{d}m \int_0^{L} \mathrm{d}L \int_0^{1} \mathrm{d}x \int_{-\infty}^{+\infty} \mathrm{d}^2 v_{lent}$$

$$\int_{-\infty}^{+\infty} \mathrm{d}^2 v_S \times \frac{\mathrm{P}(m)}{\sqrt{m}} \, v_\perp \, \nu_s(L)L^{3.5}\rho(xL)\sqrt{x(1-x)} \qquad (A22)$$

This integral has six non-independent variables, only the mass can be separated. The Monte-Carlo integration method (see Press et al. 1992) does not rely on any discretization of the integration domain, and is hence suitable for this kind of integral. Moreover, the Monte-Carlo process provides a set of simulated microlensing events, from which the time distribution can be recovered easily. The adjunction of the experimental efficiency is also straightforward with a rejection algorithm.

References

Adams, F. and Laughlin, G., 1996, ApJ 468, 586

Alard, C., 1997 A&A 321, 424

Alcock, C. et al., 1993, Nature 365, 621

Alcock, C. et al., 1995, Phys. Rev. Lett. 74, 2867

Alcock, C. et al., 1996, Nucl. Phys. Proc. Suppl. 51B, 131

Alcock, C. et al., 1997, ApJ 479, 119

Ansari et al., (EROS Collaboration), 1996, A&A 314, 94

Aubourg, E. et al., 1993, Nature 365, 623

Bahcall, J., 1984a, ApJ 287, 926

Bahcall, J., 1984b, ApJ 276, 169

Bahcall, J., 1986, ARA&A 24, 577

Bahcall, J., Flynn, C., and Gould, A., 1992, ApJ 389, 234

Bahcall, J. and Soneira, R., 1980, ApJS 44, 73

Bahcall, J. N., Soneira, R. M., and Schmidt, M., 1983, ApJ 265, 730

Baraffe, I., Chabrier, G., Allard, F., and Hauschildt, P., 1995, ApJ 446, L35

Baraffe, I., Chabrier, G., Allard, F., and Hauschildt, P., 1997, A&A 327, 1054

Beers, T. and Sommer-Larsen, J., 1995, ApJS 96, 175

Bienaymé, O., Robin, A., and Crézé, M., 1987, A&A 180, 94

Binney, J. and Tremaine, S., 1987, Galactic dynamics, Princeton University Press

Bissantz, N., Englmaier, P., Binney, J., and Gerhard, O., 1996 MN-RAS, submitted (preprint astro-ph/9612026)

Caldwell, J. and Ostriker, J., 1981, ApJ 251, 61

Carr, 1994, ARA&A, 32, 531

Casertano, S. and van Albada, S., 1990, in Lynden-Bell and Gilmore (eds.), Baryonic dark matter, Kluwer

Chabrier, G., Baraffe, I., and Plez, B., 1996a, ApJ 459, L91

Chabrier, G. and Méra, D., 1997, A&A 328, 83

Chabrier, G. and Baraffe, I., 1997, Proc. IAU Symposium #189, *Fundamental Stellar Properties: the interaction between observation and theory*, eds. T.R. Bedding, A.J. Booth and J. Davis (Kluwer; Dordrecht).

Chabrier, G., Segretain, L., and Méra, D., 1996b, ApJ 468, L21

Copi, C., Schramm, D., and Turner, M., 1995, Science 267, 192

Dahn, C., Liebert, J., Harris, H., and Guetter, H., 1995, in C. Tinney (ed.), The bottom of the main sequence - and beyond, p. 239, ESO, Springer-Verlag, Berlin

Della Valle, M. and Livio, M., 1996, ApJ 457, L77

Duquennoy, A. and Mayor, M., 1991, A&A 248, 485

Fall, S. and Rees, M., 1985, ApJ 298, 18

Fich, M. and Tremaine, S., 1991, ARA&A 29, 409

Flynn, C. and Freeman, K., 1993, A&AS 97, 835

Flynn, C. and Fuchs, B., 1994, MNRAS 270, 471

Flynn, C., Gould, A., and Bahcall, J., 1996, ApJ 466, L55

Frenk, C. and White, S., 1980, MNRAS 193, 295

Gates, E. I., Gyuk, G., and Turner, M. S., 1995, ApJ 449, L123

Gilmore, G. and Reid, N., 1983, MNRAS 202, 1025

Gilmore, G., Wyse, R., and Kuijken, K., 1989, ARA&A 27, 555

Gould, A., 1990, MNRAS 244, 25

Gould, A., Bahcall, J., and Flynn, C., 1996, ApJ 465, 759

Gould, A., Bahcall, J., and Flynn, C., 1997, ApJ, 482, 913

Graff, D. and Freese, K., 1996, ApJ 467, L65

Graff, D. and Freese, K., 1996, ApJ 456, L49

Griest, K., 1991, ApJ 366, 412

Han, C. and Gould, A., 1995, ApJ 447, 53

Han, C. and Gould, A., 1996, ApJ 467, 540

Han, C., 1997, ApJ 484, 000

Harris, W. and Racine, R., 1979, ARA&A 17, 241

Hartwick, F. and Sargent, W., 1978, ApJ 221, 512

Holtzman, J., et al., 1993, AJ 106(5), 1826

Ibata, R. and Gilmore, G., 1995, MNRAS 275, 6051

Kent, S., 1992, ApJ 387, 181

Kerins, E. J., 1995, MNRAS 276, 785

King, I., Sosin, C., and Cool, A., 1995, ApJ, 452, L33

Kiraga, M. and Paczyński, B., 1994, ApJ 430, L101

Kochanek, C., 1996, ApJ 457, 228

Kroupa, P., 1995, ApJ 453, 358

Kroupa, P., Tout, C. and Gilmore, G., 1990, MNRAS 244, 76

Kroupa, P., Tout, C. and Gilmore, G., 1993, MNRAS 262, 545

Kuijken, K. and Gilmore, G., 1989a, MNRAS 239, 571

Kuijken, K. and Gilmore, G., 1989b, MNRAS 239, 605

Kuijken, K. and Gilmore, G., 1989c, MNRAS 239, 650

Kuijken, K. and Gilmore, G., 1991, ApJ 367, L9

Kuijken, K. and Tremaine, S., 1994, ApJ 421, 178

Leggett, S., 1992, ApJS 82, 351

Layden, A. C., Hanson, R.B., Hawley, S.L., Klemola, A.R., and Hanley, C.J, 1996, ApJ 112, 2110

Lequeux, J., Fort, B., Dantel-Fort, M., Cuillandre, J.-C., and Mellier, Y., 1996, A&A 312, L1

Liebert, J., Dahn, C., and Monet, D., 1988, ApJ 332, 891

Mazeh, T., Latham, D., & Stefanik 1996 ApJ 466, 415

Méndez, R., Minniti, D., de Marchi, G., Baker, A., and Couch, W., 1996, MNRAS 283, 666

Méra, D., 1997, in preparation

Méra, D., Chabrier, G., and Baraffe, I., 1996a, ApJ 459, L87

Méra, D., Chabrier, G., and Schaeffer, R., 1996b, Europhysics Letters 33(4), 327

Méra, D., Chabrier, G., and Schaeffer, R., 1997, A&A, Paper II

Merrifield, M., 1992, AJ 103, 1552

Miller, G. and Scalo, J., 1979, ApJ, 41, 513

Monet, D., Dahn, C., Vrba, F., Harris, H., Pier, J., Luginbuhl, C., and Ables, H., 1992, AJ, 103, 638

Oort, J., 1960, Bull. Astron. Inst. Netherlands 15, 45

Ostriker, J. and Peebles, P., 1973, ApJ, 186, 467

Pacziński, B., Stanek, K. Z., Udalski, A., Szymanski, M., Kaluzny, J., Kubiak, M., and Mateo, M., 1994, AJ, 107, 2060

Paczyński, B., 1986, ApJ, 304, 1

Paczyński, B., Stanek, K., Udalski, A., Szymański, M., Kaluzny, Kubiak, M., Mateo, M., Krzemiński, W., and Preston, G., 1996, in

L. Blitz (ed.), Unsolved Problems of the Milky Way, Vol. 169 de IAU Symposium, preprint, in press

Peebles, P., 1989, ApJ, 344, L53

Peebles, P., 1990, ApJ, 362, 1

Peebles, P., 1994, ApJ 429, 43

Press, W., Teukolsky, S., Vetterling, W., and Flannery, B., 1992, Numerical Recipes, second edition, Cambridge University Press

Reid, I., Yan, L., Majewski, S., Thompson, I., and Smail, I., 1996, AJ 112, 1472

Renault, C. et al., 1997, preprint astro-ph/9612102, submitted to A&A

Richer, H. and Fahlman, G., 1992, Nature 358, 383

Sackett, P., Morisson, H., Harding, P., and Boroson, T., 1994, Nature 370, 441

Schechter, P.L., Aaronson,M., Cook,K.H.,Blanco, V.M., 1989, The Outer Galaxy Blitz and Lockman Eds, Springer

Stanek, K.Z., et al., 1997, ApJ 477, 163

Stobie, R., Ishida, K., and Peacock, J., 1989, MNRAS 238, 709

Tinney, C., Mould, J., and Reid, I., 1992, ApJ 396, 173

Udalski, A., Szymański, M., Stanek, K., Kaluzny, J., Kubiak, M., Mateo, M., Krzemiński, W., Paczyński, B., and Venkat, R., 1994, Acta Astronomica 44, 165

Wielen, R., Jahreiss, H., and Krüger, R., 1983, IAU Colloq. #76, p. 163

Zhao, H., 1994, Ph.D. thesis, Columbia Univ.

Zhao, H., Spergel, D., and Rich, R., 1995, ApJ 440, L13

Zhao, H., Spergel, D., and Rich, R., 1996, MNRAS 282, 175